The Hubble Tension as an Inference-Bias Signal: Dark Sirens with Modified Gravitational-Wave Propagation

Aiden B Smith Independent Researcher **E-mail:** aidenblakesmithtravel@gmail.com

Abstract
The Hubble tension is commonly interpreted as a mismatch in expansion history between early- and late-universe probes. If gravitational-wave (GW) luminosity distances deviate from electromagnetic distances through modified propagation, then applying a GR standard ruler introduces an inference bias in H_0. Motivated by the recently reported GWTC-3 dark-siren propagation posterior, treated here as a phenomenological template, we propagate this effect through a Planck-facing modified-gravity recalibration and obtain $H_0^{\rm Planck,MG} = 68.0$, $\Omega_m^{\rm Planck,MG} = 0.306$, and $A_{\rm lens} = 1.04$.
GR standard-ruler inversion of MG-consistent draws yields a tension-scale shift: mean $\Delta H_0 = +1.9$ km s^{-1} Mpc^{-1} for fixed Ω_m and $+4.6$ km s^{-1} Mpc^{-1} for a lensing-proxy Ω_m. Direct late-time friction closure is smaller ($\mathcal{R}^{\rm GR}_{\rm anchor} = 0.155$). Baseline CAMB projection predicts suppressed CMB lensing, while an MG-aware response refit restores near-reference quality (median $\chi^2 = 8.1$ versus 9.0 for the Planck reference). An amplitude dial, $R_\alpha(z) = 1 + \alpha\,[R(z) - 1]$, indicates cross-channel consistency near $\alpha \simeq 0.6$, whereas material relief at 0.30 would require $\alpha \simeq 2$ under linear coupling.
Within the tested nuisance families, the dark-siren preference remains positive under bounded selection-function deformations and catalogue/photo-z stresses.
This paper is an implications analysis: if a propagation deviation of this form is confirmed, corrected dark-siren inference aligns with a Planck-like anchor and GR propagation is not a neutral assumption in standard-siren cosmology.

Keywords: cosmology: theory, gravitational waves, cosmological parameters, distance scale

1 Introduction

The Hubble-constant tension between late-time distance-ladder measurements and early-universe CMB inference remains a central unresolved issue in precision cosmology [2, 10, 15]. The standard interpretation is a genuine discrepancy in expansion history. Here we test a different possibility: part of the tension is an *inference bias* generated by applying GR compression to data that follow modified-gravity (MG) propagation.

Motivated by the GWTC-3 dark-siren propagation anomaly reported in our O3 analysis release [17], this paper quantifies the cosmological parameter bias that would be induced if the inferred propagation history is physical. The propagation posterior is used as a phenomenological template; establishing its origin and robustness against catalogue/selection and waveform systematics is treated as a separate problem. Modified GW propagation with an evolving effective Planck mass has long been studied as a viable MG signature [6, 13].

In scalar-tensor/EFT constructions, the same running effective Planck mass $M_\star(z)$ that modifies GW amplitudes can also affect background and lensing channels [7, 14]. Three questions are addressed: how much late-time relief remains after recalibrating the sound-horizon anchor; whether Planck 2018 lensing necessarily rejects the implied suppression or can be accommodated by MG response freedom; and how large a GR standard-ruler inversion bias in H_0 is induced when MG truth is assumed.

2 Methodology

Posterior draws from the O3 propagation template are propagated through four linked computations. First, a 60-restart Planck+MG recalibration establishes an updated sound-horizon anchor. Secondly, constrained transfer sweeps are rebased to that anchor and recompressed into a final relief posterior. Thirdly, draw-level CAMB projection to the Planck 2018 lensing bandpowers is performed, followed by an MG-aware two-parameter lensing response refit. Finally, the GR standard-ruler inversion of $\theta_\star = r_d/D_M(z_\star)$ is applied under fixed-Ω_m and lensing-proxy-Ω_m assumptions to isolate the model-assumption bias. These are targeted cosmological forecasts and refits, not a full MG TT/TE/EE perturbation-likelihood analysis.

3 Results

3.1 Recalibrated sound-horizon anchor

The 60-restart Planck+MG run completed all restarts with 5 converged minima and 55 max-evaluation exits. Using converged minima only, we obtain:

$$\begin{aligned} H_0^{\mathrm{Planck,MG}} &= 68.01 \text{ (p50)}, \\ \Omega_m^{\mathrm{Planck,MG}} &= 0.3064 \text{ (p50)}, \\ A_{\mathrm{lens}} &= 1.043 \text{ (p50)}. \end{aligned} \tag{1}$$

With local reference $H_0^{\mathrm{local}} = 73.0$, the baseline gap used in rebased relief calculations is

$$\Delta H_0^{\mathrm{base}} = \left| H_0^{\mathrm{local}} - H_0^{\mathrm{Planck,MG}} \right| = 4.99. \tag{2}$$

3.2 Inference bias from GR standard-ruler inversion

To isolate model-assumption bias, we treat MG posterior draws as truth and invert $\theta_\star = r_d/D_M(z_\star)$ with a GR compression model. For fixed $\Omega_m = \Omega_m^{\mathrm{Planck,MG}}$, we obtain $H_{0,\mathrm{inferred}}$ mean 72.39 (p50 73.17), corresponding to

$$\Delta H_0^{\text{fixed } \Omega_\mathrm{m}} = +1.88 \text{ km s}^{-1} \text{ Mpc}^{-1} \quad \text{(mean)}. \tag{3}$$

Allowing a lensing-proxy Ω_m draw consistent with the induced H_0–Ω_m degeneracy, we obtain a larger bias,

$$\Delta H_0^{\text{lensing proxy}} = +4.55 \text{ km s}^{-1} \text{ Mpc}^{-1} \quad \text{(mean)}. \tag{4}$$

In physical terms, GR inversion acts as an *invisible wedge*: it pushes inferred anchors upward when the underlying propagation is MG-like.

Relative to the recalibrated Planck+MG anchor $H_0^{\mathrm{Planck,MG}} = 68.01$, the posterior medians shift by:

$$\begin{aligned} \Delta H_0^{\mathrm{truth}} &\approx +2.39, \\ \Delta H_0^{\text{fixed inversion}} &\approx +5.16, \\ \Delta H_0^{\text{lensing inversion}} &\approx +7.22 \text{ km s}^{-1} \text{ Mpc}^{-1}. \end{aligned} \tag{5}$$

3.3 Direct friction relief and late-time rebasing

After rebasing constrained transfer sweeps to the updated sound-horizon calibration anchor and applying Monte Carlo calibration:

$$\mathcal{R}_{\mathrm{anchor}}^{\mathrm{GR}} = 0.155. \tag{6}$$

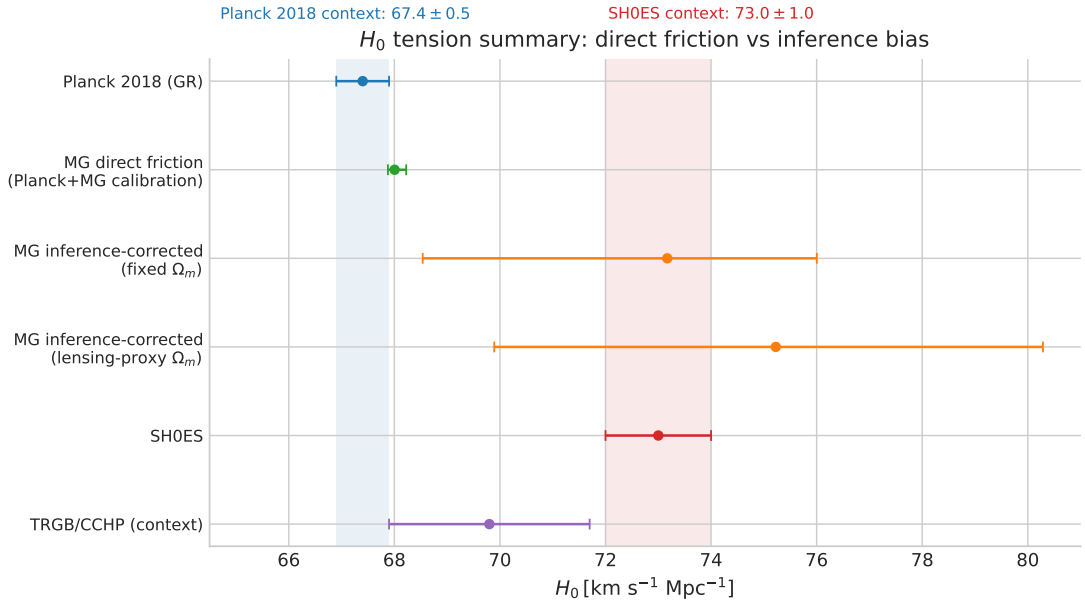

Figure 1. H_0 tension summary comparing Planck 2018 (GR), direct-friction recalibration, two GR-inversion bias channels, and local-distance-ladder context (SH0ES and TRGB/CCHP [10, 15]). The dominant displacement comes from GR standard-ruler inversion bias when MG truth is assumed; the broad lensing-proxy interval is the expected H_0–Ω_m degeneracy once the artificial ΛCDM standard-ruler rigidity is relaxed.

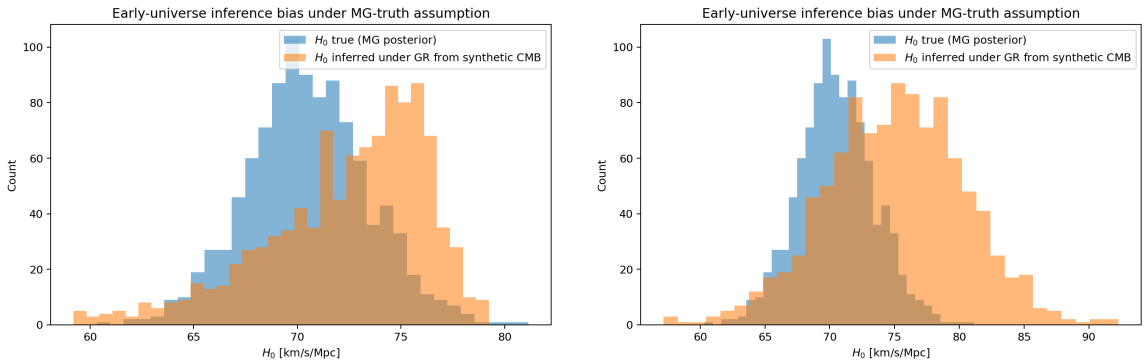

Figure 2. Draw-level H_0 truth versus GR-inferred H_0 under compressed standard-ruler inversion with fixed-Ω_m (left) and lensing-proxy-Ω_m (right). Both assumptions bias inferred H_0 upward, with larger displacement in the lensing-proxy case.

The corresponding posterior summary is p16/p50/p84 = 0.108/0.147/0.189.

Two independent robustness and joint-fit diagnostics are as follows. A 10-case robustness grid gives posterior-shift relief mean 0.530 (p50 0.513, p84 0.545), with zero failed cases. A joint SN+BAO+CC transfer fit gives relief posterior mean 0.833 (p50 0.839), but

$$\log \mathrm{BF}_{\text{transfer/no-transfer}} = -0.53, \tag{7}$$

so explicit transfer terms are not favoured in this setup. The high-z transfer-bias sensitivity map used for calibration has been moved to supplemental material (Fig. S1).

3.4 CMB lensing: baseline suppression and MG-aware response freedom

Before turning to the lensing-reconstruction likelihood, we perform a primary-spectrum closure check by fixing the phenomenological lensing-amplitude parameter A_{L} in Planck 2018 TT/TE/EE+lowE and minimising the likelihood. Relative to $A_{\mathrm{L}} = 1$, we find that $A_{\mathrm{L}} = 1.043$ (the Planck+MG median used throughout this paper) improves the best-fit primary-CMB fit by $\Delta\chi^2 = -3.46$ (best-fit $H_0 = 67.74$), and $A_{\mathrm{L}} = 1.11$ improves by $\Delta\chi^2 = -5.76$ (best-fit $H_0 = 68.15$). This is consistent with Planck's known preference for $A_{\mathrm{L}} > 1$ in the primary spectra [2] and indicates that the level of lensing-response freedom invoked below is not excluded by TT/TE/EE alone.

Baseline draw-level CAMB projection against Planck 2018 lensing bandpowers (`consext8`, 64 draws) gives:

$$\chi^2_{\text{baseline MG}} = 9.77 \quad \text{(median)}, \tag{8}$$

where the Planck reference in this bandpower window is $\chi^2_{\text{ref}} = 9.04$. The baseline mismatch is driven by an amplitude suppression of order 10–20% in $C_L^{\phi\phi}$ around $L \simeq 100$.

To test whether this baseline mismatch is rigid, we perform an MG-aware lensing refit (32 draws) with a phenomenological effective-$M_\star^2$ amplitude plus ℓ-tilt response. This freedom is motivated by scalar-tensor/EFT treatments where matter-growth and light-deflection responses need not track identically and can acquire scale dependence [7, 14]. The refit removes the baseline mismatch:

$$\chi^2_{\text{MG refit}} = 8.06 \quad \text{(median)}, \tag{9}$$

restoring near-reference quality without extreme parameter excursions.

3.5 Amplitude dial

We define a simple amplitude dial

$$R_\alpha(z) = 1 + \alpha\,[R(z) - 1], \tag{10}$$

and evaluate cross-channel support using existing growth, lensing, and distance-ratio consistency summaries as a fast emulator (not a full re-inference at each α). We find: the distance-ratio criterion passes at $\alpha \approx 0.18$; the growth criterion passes at $\alpha \approx 0.58$; the lensing-growth consistency criterion passes at $\alpha \approx 0.60$; and the combined support criterion (M2) turns on at $\alpha \approx 0.60$. For the material-relief requirement ($\mathcal{R}^{\mathrm{GR}}_{\text{anchor}} \geq 0.30$), two cases are informative: (i) if relief is held fixed at the current calibrated level, no solution appears for $\alpha \in [0, 3]$; (ii) under linear relief coupling, $\mathcal{R}_{\text{anchor}}(\alpha) \propto \alpha$, the threshold is crossed at $\alpha \approx 1.95$. This gives a simple

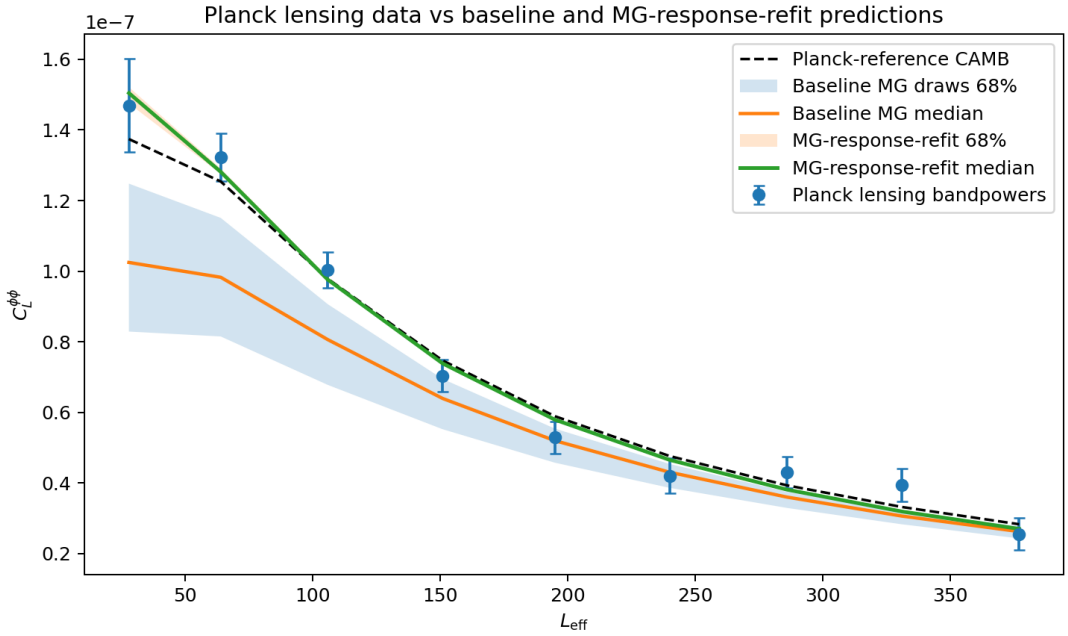

Figure 3. Planck 2018 lensing bandpowers with baseline MG projection and MG-aware refit overlay. The refit absorbs the baseline suppression and restores near-reference fit quality.

scale estimate: core cross-channel support is compatible with the present signal level, while material closure needs roughly a factor-of-two stronger effective propagation amplitude under linear coupling.

3.6 Cross-probe and stability checks

We ran a public-data robustness package based on re-scoring cached O3 dark-siren likelihood terms (the injection-logit selection-calibrated configuration). The aim is to confront the dominant escape hatches: selection-function misspecification, galaxy-catalogue/photo-z biases, and PE analysis dependence, and to test for coherent redshift scaling of the preference.

Adversarial selection-function deformation. We deform the injection-calibrated detection efficiency with bounded multiplicative splines in effective SNR (five knots) and redshift (three knots), plus a mild mass-tilt term, and then perform constrained adversarial minimisation of ΔLPD with explicit regularisation. Across bounds spanning $\pm 10\%$ to $\pm 60\%$ deformations in this nuisance family, the best-achieved score remains essentially unchanged at $\Delta\mathrm{LPD} \simeq +3.67$; no tested bound drives the preference below 1 or 0.

Catalogue/photo-z stress in the dominant spectral channel. Using spectral-only rescoring (which retains most of the baseline preference), we apply global perturbations to the top-N high-leverage events covering $\simeq 80\%$ of the baseline score with a simple redshift-bias model $\Delta z = b_0 + b_1 z$ and a bounded completeness-weight tilt. Even extreme grid choices (e.g. $b_0 = 0.03$, $b_1 = 0.2$) reduce but do not erase the signal, giving $\Delta\mathrm{LPD} \simeq +1.98$; completeness-weight deformations at the $\pm 20\%$ level leave $\Delta\mathrm{LPD} \gtrsim +3.61$.

Spectroscopic redshift override (direct photo-z stress). To attack the dominant remaining catalogue escape hatch more directly, we identify the top-K host candidates per high-leverage event under the same host-weight proxy used in spectral-only scoring, crossmatch their sky coordinates against public spectroscopic redshift resources (2MRS, 6dFGS, 2dFGRS, GAMA DR3, SDSS DR16 spectroscopy, and DESI DR1), and override the catalogue redshift with $z_{\rm spec}$ where available. With DESI included, at $(r, K) = (30'', 20000)$ this anchors $\simeq 9\%$ (GW200308_173609), $\simeq 5\%$ (GW200220_061928), and $\simeq 10\%$ (GW200219_094415) of the total host-weight proxy to spectroscopic redshifts (other high-leverage events remain at the percent level or below at current footprint overlap), with median matched host-weight fraction $\simeq 5\%$. The score is stable or slightly higher: $\Delta\mathrm{LPD}_{\rm tot}$ rises from 3.63 (baseline) to 3.65 under the override (e.g. 3.64 at $r = 3''$ and 3.65 at $r = 30''$), under unchanged selection normalisation. Across the (r, K) grid, $\Delta\mathrm{LPD}_{\rm tot}$ is non-decreasing with spec-z weight coverage (pooled slope $b \simeq 0.40$, $p \simeq 10^{-10}$, i.e. $\approx 4 \times 10^{-3}$ per $+1\%$ coverage). Shifted-sky false-match controls show that coincidence rates rise rapidly with match radius once dense spec-z catalogues are included: $r = 60''$ is coincidence-dominated (median shifted/true $\simeq 0.72$ and excluded by the gate), while $r = 3''$ remains clean (median shifted/true $\simeq 2 \times 10^{-3}$) and $r = 10''$ remains low-coincidence (median shifted/true $\simeq 0.05$). We therefore treat $r \leq 10''$ as the conservative regime for this spec-z override audit.

PE analysis-group swaps for high-leverage events. For GW200308_173609 and GW200220_061928, we rebuild the binned (Ω, d_L) posterior using alternative GWTC-3 PEDataRelease analysis groups (C01:Mixed, C01:IMRPhenomXPHM, C01:SEOBNRv4PHM) while matching the baseline histogram support. In spectral-only rescoring, the global preference is stable at $\Delta\mathrm{LPD} \approx +3.63$ across these choices.

Redshift scaling. Using the luminosity-distance posterior median to form three equal-count bins, the preference concentrates at higher distance: $\Delta\mathrm{LPD} \approx -0.52$, $+0.57$, and $+3.55$ from low to high bins. This monotonic concentration is qualitatively consistent with a cumulative propagation effect and provides a falsifiable scaling target for larger siren samples.

Redshift-scramble null. To test whether the preference depends on coherent catalogue redshift structure in the dominant spectral channel, we compress each event's galaxy term into a binned redshift-weight histogram (spectral-only) and randomly permute the bin weights while holding the PE distance posterior, missing-host term, and selection normalisation fixed. In this null, the data-only contribution shifts from $\Delta\mathrm{LPD}_{\rm data} \simeq +2.65$ to a null mean $+2.27 \pm 0.13$, with empirical tail probability $p \simeq 0.025$; the total score weakens similarly ($p \simeq 0.05$). The preference therefore degrades under redshift scrambling, but does not collapse to zero in this fast binned-z approximation.

Pantheon inference-bias audit. In an SN-only transfer model, we obtain a weak same-sign preference for transfer terms:

$$\log \mathrm{BF}_{\rm transfer/no\text{-}transfer} \approx +0.24. \tag{11}$$

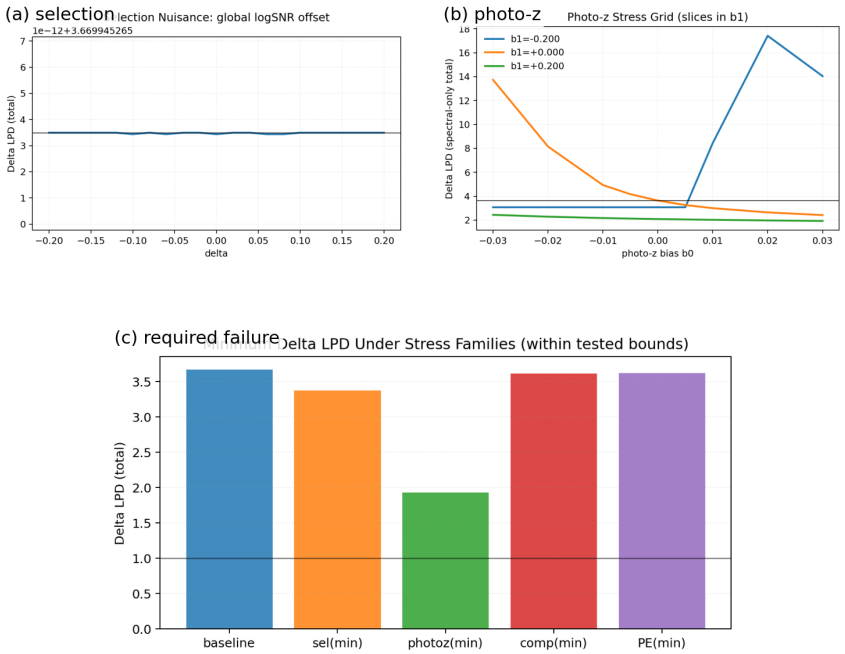

Figure 4. Dark-siren robustness summary from public-data re-scoring: selection-function adversarial deformation, photo-z/completeness stress (dominant spectral channel), and the minimum ΔLPD reached within tested nuisance families.

In the all-transfer variant (SN+BAO+CC+ladder term), the score is mildly negative:

$$\log \mathrm{BF}_{\text{transfer/no-transfer}} \approx -0.48. \tag{12}$$

This is compatible with a small inference-bias contribution in SN-only compression, but not a decisive multi-probe detection at current calibration depth.

High-leverage-event jackknife stability. For the O3 selection-function-calibrated configuration, the full score is

$$\Delta\mathrm{LPD}_{\text{full}} = 3.67. \tag{13}$$

Dropping the highest-leverage event (GW200308_173609) gives

$$\Delta\mathrm{LPD}_{\text{drop 1}} = 2.19, \tag{14}$$

and an approximate top-2 leave-out gives

$$\Delta\mathrm{LPD}_{\text{drop 2}} \approx 1.70. \tag{15}$$

The signal is therefore concentrated in a small subset of high-leverage events, but it does not collapse when the top event is removed.

Nonlinear bridge scan. Using a late-transition profile

$$\alpha(z) = \alpha_{\text{high}} + \frac{\alpha_{\text{low}} - \alpha_{\text{high}}}{1 + \exp[(z - z_t)/w]}, \tag{16}$$

we find broad viable families that satisfy growth/lensing consistency near $\alpha_{\text{eff}} \sim 0.6$ while reaching material-relief targets near $\alpha_{\text{relief,eff}} \sim 1.94$ to 1.95 in low-z windows. A representative solution is

$$(\alpha_{\text{high}}, \alpha_{\text{low}}, z_t, w) \approx (0.60, 1.95, 0.26, 0.03), \tag{17}$$

with comparable neighbouring solutions for other low-z effective windows.

Entropy-anchored direct dark-siren re-score. We also replaced the phenomenological propagation posterior with the entropy-reconstruction posterior from the submission-hardening run and re-scored the same O3 selection-function-calibrated dark-siren set. The total support remains positive but is reduced:

$$\Delta\mathrm{LPD}_{\text{entropy direct}} = 2.26 \quad \text{(vs. 3.67 baseline)}. \tag{18}$$

The same highest-leverage event remains GW200308_173609; leave-one-out gives

$$\Delta\mathrm{LPD}_{\text{entropy, drop GW200308}} = 1.20. \tag{19}$$

Numerically this is about 0.62 of the baseline support, consistent with the entropy-alignment quick test indicating effective amplitudes below the material-relief scale.

4 Discussion and conclusions

The central result is that GR-assumed standard-ruler inversion can introduce a tension-scale inference bias in H_0 if GW propagation is modified at the level implied by the adopted template. In this framework, the induced shift is of order +2 to +5 km s^{-1} Mpc^{-1}.

Direct friction closure is smaller, with $\mathcal{R}^{\rm GR}_{\rm anchor} \simeq 0.16$. The dominant mechanism in this paper is therefore not late-time closure by friction alone, but the parameter wedge created by a mismatched inference model: GR compression can separate early and late anchors even when the underlying cosmology is internally consistent under MG truth.

This interpretation is compatible with our lensing and stability checks. Baseline lensing projection is suppressed, but MG-aware response freedom restores near-reference performance. Public-data dark-siren re-scoring indicates that within the tested nuisance families the preference remains positive under bounded selection-function deformations and catalogue/photo-z stresses. Pantheon SN-only transfer is weakly same-sign while the all-transfer variant is mildly negative, so present electromagnetic-sector evidence remains suggestive rather than decisive. Jackknife tests show concentration in GW200308_173609 and other high-leverage events, but no single-event collapse.

The identified vulnerabilities correspond to explicit, near-term tests. If the propagation deviation is physical, the population-level preference should stabilise (and should become less dominated by single events) as the siren sample grows and galaxy-catalogue completeness and selection modelling improve in O4/O5. Similarly, the degree of lensing response freedom required to reconcile baseline suppression with Planck 2018 lensing can be confronted with higher-precision CMB lensing measurements and joint large-scale-structure combinations, which should either recover a consistent MG response or exclude the relevant parameter space.

Even if the GWTC-3 propagation preference is ultimately attributed to residual systematics, the mapping derived here quantifies the magnitude of bias that would follow from a propagation deviation of comparable form, and motivates treating GR propagation as an explicit assumption to be stress-tested in standard-siren cosmology. If the signal persists in larger siren samples, corrected dark-siren inference no longer requires a universally high late-time H_0, and the remaining discrepancy is more naturally isolated to the electromagnetic calibration/propagation sector rather than to a single global expansion-history failure.

Acknowledgements

The author used AI-assisted tools for drafting, editing, and software development.

Declarations

Conflict of interest

The author declares no competing interests.

Data availability

All code and reproducibility artefacts used in this study are archived at Zenodo, DOI 10.5281/zenodo.18635659. Upstream O3 search-sensitivity injections are available at DOI 10.5281/zenodo.7890437. Public cosmological datasets used here are cited in the reference list with corresponding DOIs.

Funding
This research received no specific grant from any funding agency in the public, commercial, or not-for-profit sectors.

References

References

[1] R. Abbott *et al.* (LIGO Scientific Collaboration, Virgo Collaboration, and KAGRA Collaboration), "GWTC-3: Compact Binary Coalescences Observed by LIGO and Virgo During the Second Part of the Third Observing Run," *Phys. Rev. X* **13**, 041039 (2023), DOI: 10.1103/PhysRevX.13.041039.

[2] N. Aghanim *et al.* (Planck Collaboration), "Planck 2018 results. VI. Cosmological parameters," *Astron. Astrophys.* **641**, A6 (2020), DOI: 10.1051/0004-6361/201833910.

[3] N. Aghanim *et al.* (Planck Collaboration), "Planck 2018 results. VIII. Gravitational lensing," *Astron. Astrophys.* **641**, A8 (2020), DOI: 10.1051/0004-6361/201833886.

[4] S. Alam *et al.*, "The clustering of galaxies in the completed SDSS-III Baryon Oscillation Spectroscopic Survey: cosmological analysis of the DR12 galaxy sample," *Mon. Not. R. Astron. Soc.* **470**, 2617 (2017), DOI: 10.1093/mnras/stx721.

[5] S. Alam *et al.*, "Completed SDSS-IV extended Baryon Oscillation Spectroscopic Survey: Cosmological implications from two decades of spectroscopic surveys at the Apache Point Observatory," *Phys. Rev. D* **103**, 083533 (2021), DOI: 10.1103/PhysRevD.103.083533.

[6] E. Belgacem, Y. Dirian, S. Foffa, and M. Maggiore, "Modified gravitational-wave propagation and standard sirens," *Phys. Rev. D* **98**, 023510 (2018), DOI: 10.1103/PhysRevD.98.023510.

[7] E. Bellini and I. Sawicki, "Maximal freedom at minimum cost: linear large-scale structure in general modifications of gravity," *J. Cosmol. Astropart. Phys.* **07** (2014) 050, DOI: 10.1088/1475-7516/2014/07/050.

[8] D. Brout *et al.*, "The Pantheon+ Analysis: Cosmological Constraints," *Astrophys. J.* **938**, 110 (2022), DOI: 10.3847/1538-4357/ac8e04.

[9] DESI Collaboration, "DESI 2024 VI: cosmological constraints from the measurements of baryon acoustic oscillations," *J. Cosmol. Astropart. Phys.* **02** (2025) 021, DOI: 10.1088/1475-7516/2025/02/021.

[10] W. L. Freedman *et al.*, "The Carnegie-Chicago Hubble Program. VIII. An independent determination of the Hubble constant based on the tip of the red giant branch," *Astrophys. J.* **882**, 34 (2019), DOI: 10.3847/1538-4357/ab2f73.

[11] LIGO Scientific Collaboration, Virgo Collaboration, and KAGRA Collaboration, "GWTC-3: Compact Binary Coalescences Observed by LIGO and Virgo During the Second Part of the Third Observing Run — O3 search sensitivity estimates," Zenodo (2023), DOI: 10.5281/zenodo.7890437.

[12] M. Moresco *et al.*, "Improved constraints on the expansion rate of the Universe up to $z \sim 1.1$ from the spectroscopic evolution of cosmic chronometers," *J. Cosmol. Astropart. Phys.* **08** (2012) 006, DOI: 10.1088/1475-7516/2012/08/006.

[13] A. Nishizawa, "Generalized framework for testing gravity with gravitational-wave propagation," *Phys. Rev. D* **97**, 104037 (2018), DOI: 10.1103/PhysRevD.97.104037.

[14] L. Pogosian and A. Silvestri, "What can cosmology tell us about gravity? Constraining Horndeski gravity with Σ and μ," *Phys. Rev. D* **94**, 104014 (2016), DOI: 10.1103/PhysRevD.94.104014.

[15] A. G. Riess *et al.*, "A Comprehensive Measurement of the Local Value of the Hubble Constant with 1 km s^{-1} Mpc^{-1} Uncertainty from the Hubble Space Telescope and the SH0ES Team," *Astrophys. J. Lett.* **934**, L7 (2022), DOI: 10.3847/2041-8213/ac5c5b.

[16] J. Simon, L. Verde, and R. Jimenez, "Constraints on the redshift dependence of the dark energy potential," *Phys. Rev. D* **71**, 123001 (2005), DOI: 10.1103/PhysRevD.71.123001.

[17] A. B. Smith, "O3 Modified Gravity Tension Replication," Zenodo (2026), DOI: 10.5281/zenodo.18635659.

[18] D. Stern *et al.*, "Cosmic chronometers: constraining the equation of state of dark energy. I: $H(z)$ measurements," *J. Cosmol. Astropart. Phys.* **02** (2010) 008, DOI: 10.1088/1475-7516/2010/02/008.